BELLE2-CONF-PH-2022-XXX
March 2, 2022

Measurements of the branching fraction and direct *CP*-violating asymmetry in $B^0 \to K^0\pi^0$ decays

(Belle II Collaboration)

Abstract

We report the measurements of branching fraction ($\mathcal{B}$) and direct *CP*-violating asymmetry ($\mathcal{A}_{CP}$) in the charmless decays $B^0 \to K^0\pi^0$ at Belle II. A sample of e^+e^- collisions, corresponding to $189.8\,\text{fb}^{-1}$ of integrated luminosity, recorded near the $\Upsilon(4S)$ resonance is used for the study. We find 135 signal candidates, and measure $\mathcal{B}(B^0 \to K^0\pi^0) = [11.0 \pm 1.2(\text{stat}) \pm 1.0(\text{syst})] \times 10^{-6}$ and $\mathcal{A}_{CP} = -0.41^{+0.30}_{-0.32}(\text{stat}) \pm 0.08(\text{syst})$.

1. INTRODUCTION

Decays mediated by flavour-changing neutral current transitions are suppressed in the standard model (SM) and provide an indirect route to search for beyond-the-SM physics. The latter is accomplished via a consistency check between measurements and corresponding theory predictions since new particles may enter the quantum loop [1]. Within the SM, *CP* violation arises due to an irreducible phase in the Cabibbo-Kobayashi-Maskawa (CKM) matrix [2]. At an e^+e^- flavor-factory experiment such as Belle II, neutral B meson pairs are coherently produced in the process $e^+e^- \to \Upsilon(4S) \to B^0\overline{B}^0$. When one of these B mesons decays to a *CP* eigenstate f_{CP} and the other to a flavor-specific final state $f_{\rm tag}$, the time-dependent decay rate is given as

$$\mathcal{P}(\Delta t) = \frac{e^{-|\Delta t|/\tau_{B^0}}}{4\tau_{B^0}}[1 + q\{\mathcal{A}\cos(\Delta m_d \Delta t) + \mathcal{S}\sin(\Delta m_d \Delta t)\}], \quad (1)$$

where $\Delta t = t_{CP} - t_{\rm tag}$ is the proper time difference between the decay into f_{CP} and $f_{\rm tag}$, q is the flavor of $f_{\rm tag}$ being $+1$ (-1) for the B^0 ($\overline{B}^0$) decay to $f_{\rm tag}$, Δm_d is the B^0–$\overline{B}^0$ mixing frequency, and τ_{B^0} is the B^0 lifetime. The quantity $\mathcal{A}$ is a measure of direct *CP* violation, and $\mathcal{S}$ denotes *CP* violation due to interference between decays with and without B^0–$\overline{B}^0$ mixing.

The CKM and color suppression of the tree-level $b \to su\overline{u}$ transition means that the $B^0 \to K^0_S\pi^0$ decays are dominated by the top-quark mediated $b \to sd\overline{d}$ loop diagram, which carries a weak phase $\arg(V_{tb}V^*_{ts})$; V_{ij} denote the CKM matrix elements. If subleading contributions are small, $\mathcal{S}_{K^0_S\pi^0}$ is expected to be equal to $\sin 2\phi_1$ and $\mathcal{A}_{K^0_S\pi^0} \approx 0$. Therefore, a precise measurement of the direct *CP* asymmetry ($\mathcal{A}$) and branching fraction ($\mathcal{B}$) in this decay channel represents an important consistency test of the SM. Furthermore, $B^0 \to K^0_S\pi^0$ is a key component in improving the sensitivity of an isospin sum-rule proposed by Gronau [3]. The sum rule, given by

$$I_{K\pi} = \mathcal{A}_{K^+\pi^-} + \mathcal{A}_{K^0\pi^+}\frac{\mathcal{B}(K^0\pi^+)}{\mathcal{B}(K^+\pi^-)}\frac{\tau_{B^0}}{\tau_{B^+}} - 2\mathcal{A}_{K^+\pi^0}\frac{\mathcal{B}(K^+\pi^0)}{\mathcal{B}(K^+\pi^-)}\frac{\tau_{B^0}}{\tau_{B^+}} - 2\mathcal{A}_{K^0\pi^0}\frac{\mathcal{B}(K^0\pi^0)}{\mathcal{B}(K^+\pi^-)} = 0, \quad (2)$$

properly accounts for subleading amplitudes by combining the $\mathcal{B}$ and $\mathcal{A}$ values measured in B decays to all four $K\pi$ final states: $K^+\pi^-$, $K^0\pi^+$, $K^+\pi^0$, and $K^0\pi^0$. The rule offers a stringent null test of the SM. The impact of Belle II's inputs on the $I_{K\pi}$ determination [4] is evident from Fig. 1 with the dominant uncertainty arising from the $\mathcal{A}_{K^0\pi^0}$ measurement. Previous measurements of *CP* violation in $B^0 \to K^0\pi^0$ decay have been reported by Belle and BaBar [5–8]. With the data size anticipated at Belle II, we expect to have significantly smaller uncertainties compared to what Belle and BaBar have achieved for these quantities.

In this document, we report the measurements of $\mathcal{B}$ and $\mathcal{A}_{CP}$ in $B^0 \to K^0\pi^0$ decays at Belle II conducted using a time-dependent analysis framework. Owing to the limited statistics, we are unable to simultaneously measure $\mathcal{A}_{CP}$ and $\mathcal{S}_{CP}$; instead we fix the latter to its world-average value [9].

2. THE BELLE II DETECTOR AND DATA SAMPLES

Belle II [10] is a particle spectrometer with almost 4π solid-angle coverage, designed to reconstruct the final-state particles of e^+e^- collisions produced by the SuperKEKB

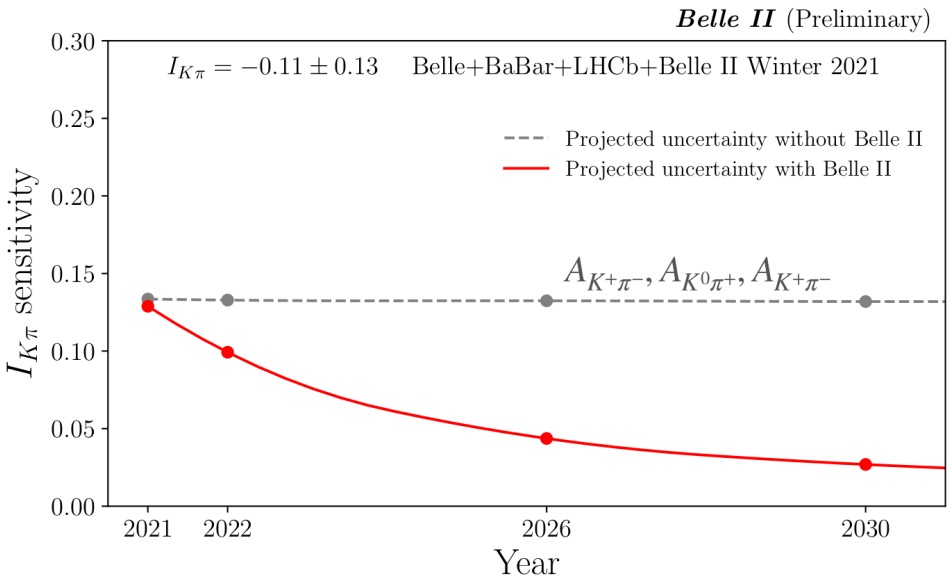

FIG. 1. The projected uncertainty on $I_{K\pi}$ with and without Belle II inputs.

asymmetric-energy collider [11], located at the KEK laboratory in Tsukuba, Japan. The energies of the electron and positron beams are 7 GeV and 4 GeV, respectively. Belle II comprises several subdetectors surrounding the interaction point in a cylindrical geometry. The innermost subdetector is the vertex detector (VXD), which uses position-sensitive silicon layers to sample the trajectories of charged particles (tracks) in the vicinity of the interaction region to extrapolate the decay positions of their long-lived parent particles. The VXD includes two inner layers of DEPFET-based pixel sensors and four outer layers of double-sided silicon microstrip sensors. The second pixel layer is currently incomplete covering only one sixth of the azimuthal angle. Charged-particle momenta and charges are measured by a large-radius, helium-ethane, small-cell central drift chamber (CDC), which also offers charged-particle-identification information via a measurement of specific ionization. A Cherenkov-light angle and time-of-propagation (TOP) detector surrounding the CDC provides charged-particle identification in the central detector volume, supplemented by proximity-focusing, aerogel, ring-imaging Cherenkov (ARICH) detectors in the forward region with respect to the electron beam. A CsI(Tl)-crystal electromagnetic calorimeter (ECL) provides electron-energy measurements and photon reconstruction. A solenoid surrounding the calorimeter generates a uniform axial 1.5 T magnetic field filling its inner volume. Layers of plastic scintillators and resistive-plate chambers, interspersed between the magnetic flux-return iron plates, allow for the identification of K_L^0 and muons. The subdetectors most relevant for this study are the VXD, CDC, and ECL.

The data sample used in the study consists of all good-quality runs collected at a center-of-mass (CM) energy at the $\Upsilon(4S)$ resonance, corresponding to an integrated luminosity of $189.8\,\text{fb}^{-1}$. We use Monte Carlo (MC) simulated data to optimize the event selection and study possible background contributions. We use signal-only simulated data to determine the signal models and estimate the selection efficiency. The so-called generic MC sample consists of simulated events that include $q\bar{q}$ ($q = u, d, s, c$), $B^0\overline{B}^0$ and B^+B^- events in realistic proportions, corresponding to more than 10 times that of the $\Upsilon(4S)$ data. The latter sample is used to study background and make comparisons with the data. The

$B-$meson decays are simulated with the EvtGen generator [12] and the effect of final-state electromagnetic radiation is simulated by the Photos package [13]. The simulation of the continuum $e^+e^- \to q\overline{q}$ background process is carried out with the KKMC generator [14] interfaced to Pythia [15]. The interactions of particles with the detector are simulated using Geant4 [16].

3. RECONSTRUCTION AND SELECTION

Charged particle tracks are reconstructed with the SVD and CDC. Photons are identified as isolated ECL clusters that are not matched to any charged particle track. The K^0_S candidates are reconstructed from pairs of oppositely charged tracks having invariant mass between 482 and 513 MeV/c^2. We reconstruct π^0 candidates from pairs of photons that have energies larger than the thresholds of 80 and 223 MeV for final-state photons detected in the barrel and endcap, respectively, of the ECL. The selection also requires π^0 mass to lie between 119 and 150 MeV/c^2 and the absolute cosine of the π^0 helicity angle to be less than 0.953. These criteria suppress contributions from misreconstructed π^0 candidates.

The B-meson candidate is reconstructed by combining a K^0_S with a π^0 candidate. For this purpose, we use two kinematic variables: the beam-energy-constrained mass ($M_{\rm bc}$) and the energy difference (ΔE), defined as

$$\begin{aligned} M_{\rm bc} &= \sqrt{E^2_{\rm beam} - \vec{p}^{\,2}_B}, \\ \Delta E &= E_B - E_{\rm beam}, \end{aligned} \tag{3}$$

where $E_{\rm beam}$ is the beam energy, E_B and $\vec{p}_B$ are respectively the reconstructed energy and momentum of the B meson; all calculated in the CM frame. We retain candidate events satisfying $|\Delta E| < 0.3$ GeV and $5.24 < M_{\rm bc} < 5.29$ GeV/c^2.

The presence of a high momentum π^0 causes a nontrivial correlation between ΔE and $M_{\rm bc}$ owing to the shower leakage of final-state photons. To minimize the impact of such correlation, we introduce a modified $M'_{\rm bc}$, calculated from the beam energy and momenta of final-state particles as:

$$M'_{\rm bc} = \sqrt{E^2_{\rm beam} - \left(\vec{p}_{K^0_S} + \frac{\vec{p}_{\pi^0}}{|\vec{p}_{\pi^0}|}\sqrt{(E_{\rm beam} - E_{K^0_S})^2 - m^2_{\pi^0}}\right)^2}, \tag{4}$$

where all kinematic quantities are calculated in the CM frame. We find that the linear correlation coefficient has been reduced for all event categories with the introduction of the modified $M'_{\rm bc}$, which we will refer to as just $M_{\rm bc}$ henceforth in this document. As shown in Eq. (1), one of the most important parameters to estimate the decay rate is Δt. It is found that the error on it ($\Delta t_{\rm err}$) has a significant tail (Fig. 2), caused by the events with poor decay time resolution. We apply a selection $\Delta t_{\rm err} < 2.5$ ps to suppress such events.

The most dominant source of background is from $e^+e^- \to q\overline{q}$ ($q = u, d, s, c$) continuum process. These events result in final-state particles collimated into two back-to-back jets, whereas those from $e^+e^- \to \Upsilon(4S) \to B\overline{B}$ are uniformly distributed over the 4π solid angle. We exploit this difference in event topology to suppress the continuum background. We combine a set of 39 variables, known to provide discrimination between $B-$meson signal and continuum background, using a boosted decision tree (BDT) [17] classifier. We use $e^+e^- \to q\overline{q}$, $B^0\overline{B}^0$ and B^+B^- MC events, each equivalent to an integrated luminosity of

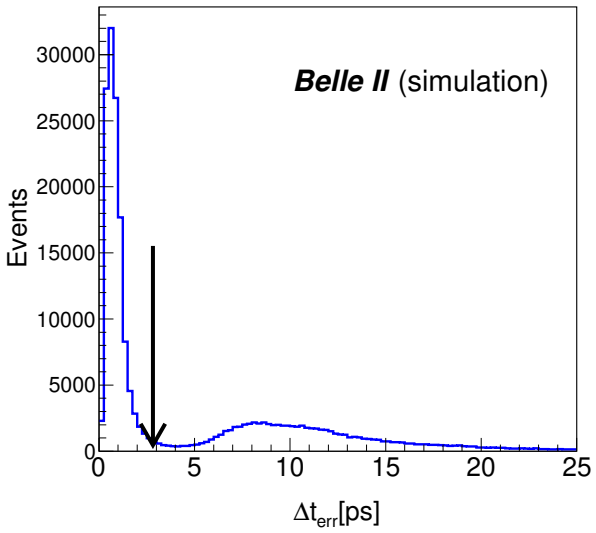

FIG. 2. Distribution of $\Delta t_{\rm err}$.

$1\,{\rm ab}^{-1}$, for this purpose. The BDT output clearly discriminate the signal from background events. As it is difficult to model the BDT output distribution ($C_{\rm out}$) analytically, we translate it into a new variable:

$$C'_{\rm out} = \ln\left(\frac{C_{\rm out} - C_{\rm out,min}}{C_{\rm out,max} - C_{\rm out}}\right), \tag{5}$$

which can be parametrized by one or more Gaussian functions. Here, $C_{\rm out,min} = 0.6$ and $C_{\rm out,max} \simeq 1$. With the $C_{\rm out,min}$ criterion, we reject about 89% of the continuum background at a 18% relative loss in signal efficiency.

After the final selection and background suppression, we find that the number of B candidates per event is 1.009. The multiple candidates mostly arises due to a random combination of final-state particles. In order to find the best candidate in events with multiple candidates, we first compare the π^0 mass-constrained fit χ^2 probability (p-value). The K^0_S vertex fit p-value is served as the second indicator of the validity of the candidate. The candidate with the larger p-value is retained as the best candidate in an event. This method retains the correct B candidate out of the events with more than one B candidates 74% of the times. The efficiency of correctly reconstructed signal events after all the selection is found to be 12.3% and the fraction of self cross-feed (SCF) events are 1.5%. As the SCF fraction is small, we consider both correctly reconstructed and SCF events as part of the signal.

The vertex position for the $B^0 \to K^0_S\pi^0$ decay is reconstructed using charged pions from the K^0_S decay and an IP constraint. The tag side vertex is obtained with well-reconstructed tracks that are not assigned to the $B^0 \to K^0_S\pi^0$ decay. The flavour of the tag side B meson is determined from properties of particles that are not associated with the reconstructed $B^0 \to K^0_S\pi^0$ decays. We use the standard Belle II flavour tagging algorithm [18] that gives two parameters, the b-flavor charge, q and its quality factor, r. We get $q = +1$ (-1) when the tagged B meson is a B^0 ($\overline{B}^0$). The parameter r is an event-by-event, MC determined flavour-tagging dilution factor that ranges from 0 (no flavour discrimination) to 1 (unambiguous flavour assignment). Each event is divided into seven r regions. We also employ the r-bin

dependent wrong tag fraction (w_r), the difference in wrong tag fraction between B^0 and $\overline{B}^0$ (Δw_r), tagging efficiency (ϵ_r), and tagging efficiency difference (μ_r) that are necessary to extract CP parameters in data.

4. SIGNAL EXTRACTION

The signal yields are obtained from a four-dimensional (4D) unbinned extended maximum-likelihood fit to ΔE, $M_{\rm bc}$, $C'_{\rm out}$, and Δt. For the signal component, ΔE is modeled with a sum of a Crystal Ball (CB) [19] and a double Gaussian function with common mean, $M_{\rm bc}$ with a sum of CB and a Gaussian function, and $C'_{\rm out}$ with a sum of bifurcated and a Gaussian functions. The Δt PDF is given by Eq. (6), where $\mathcal{R}_{\rm sig}$ is the proper time resolution function composed of a sum of double Gaussian functions, which takes the finite vertex resolution into account.

$$P_{\rm sig}(\Delta t, q) = \frac{{\rm e}^{-|\Delta t|/\tau_{B^0}}}{4\tau_{B^0}}\{[1 - q\Delta w_r + q\mu_r(1-2w_r)] + [q(1-2w_r) + \mu_r(1 - q\Delta w_r)] \quad (6)$$
$$(\mathcal{A}_{CP}\cos(\Delta m_d \Delta t) + \mathcal{S}_{CP}\sin(\Delta m_d \Delta t))\} \otimes \mathcal{R}_{\rm sig},$$

where, w_r =wrong tag fraction, Δw_r=wrong tag fraction difference, μ_r= tag efficiency difference, $\tau_{B^0} = 1.520$ ps and $\Delta m_d = 0.507$ ps^{-1}. For the continuum background component, a linear function is used to model ΔE, an ARGUS function [20] is used for $M_{\rm bc}$, and a sum of asymmetric and symmetric Gaussian functions is used to model $C'_{\rm out}$. The continuum Δt distribution is modeled with an exponential function convolved with a Gaussian for the outlier; for resolution function ($\mathcal{R}_{\rm q\bar{q}}$) we use sum of double Gaussian. For the $B\overline{B}$ background component, a two-dimensional Kernel estimation PDF [21] is used to model both ΔE and $M_{\rm bc}$ distributions, and a sum of bifurcated and a Gaussian functions is used to model $C'_{\rm out}$. The Δt distribution for the $B\overline{B}$ component is modeled with an exponential function convolved with a Gaussian for outlier; for resolution function ($\mathcal{R}_{\mathcal{B}\bar{\mathcal{B}}}$) we use sum of double Gaussian. The signal PDF shapes are fixed to the values determined from a $q \cdot r$ binned signal MC fit. The $B\overline{B}$ background shape are fixed from the overall MC fit. For the continuum background component we float the PDF shape parameters over the $q \cdot r$ bin. The free parameters in the final fit are the signal yield, $\mathcal{A}_{CP}$, (Gaussian-constrained) BB background yield, continuum background yield, ΔE slope, Argus parameter and $C'_{\rm out}$ relative width for the $q\overline{q}$ component. The $\mathcal{S}_{CP}$ value fixed to the world avarage value. We correct the ΔE, $M_{\rm bc}$ and $C'_{\rm out}$ PDF shapes for possible data-MC differences, according to the values obtained with a high-statistic control sample of $B^+ \to \overline{D}^0(\to K^+\pi^-\pi^0)\pi^+$.

We use a high-statistic control sample $B^0 \to J/\psi K^0_S$ to validate our time-dependent analysis framework. To mimic the signal decay, we do not vertex the two charged leptons coming from the J/ψ decay. The obtained values of the B^0 lifetime, $\mathcal{A}_{CP}$ and $\mathcal{S}_{CP}$ are found to be consistent with the PDG values. The same control sample is also used to correct the Δt PDF shape parameters for possible data-MC differences.

Figure 3 shows the signal-enhanced projections for the $q\cdot r$-integrated 4D fit. The obtained signal yield is 135^{+16}_{-15}, where the quoted uncertainty is statistical only. We also obtain 2214^{+49}_{-48} events for $q\overline{q}$ and 44 ± 5 events for BB backgrounds. The obtained $B^0 \to K^0\pi^0$ branching fraction is $(11.0 \pm 1.2 \pm 1.0) \times 10^{-6}$, where the first uncertainty is statistical and the second is systematic (described below). The measured direct CP-violating asymmetry is $\mathcal{A}_{CP} = -0.41^{+0.30}_{-0.32}({\rm stat}) \pm 0.08({\rm syst})$. This is an improved measurement of $\mathcal{B}$ and $\mathcal{A}_{CP}$ in

$B^0 \to K^0\pi^0$ decays compared to the previous Belle II result [22] where a time-integrated study was performed to extract the $\mathcal{A}_{CP}$ value.

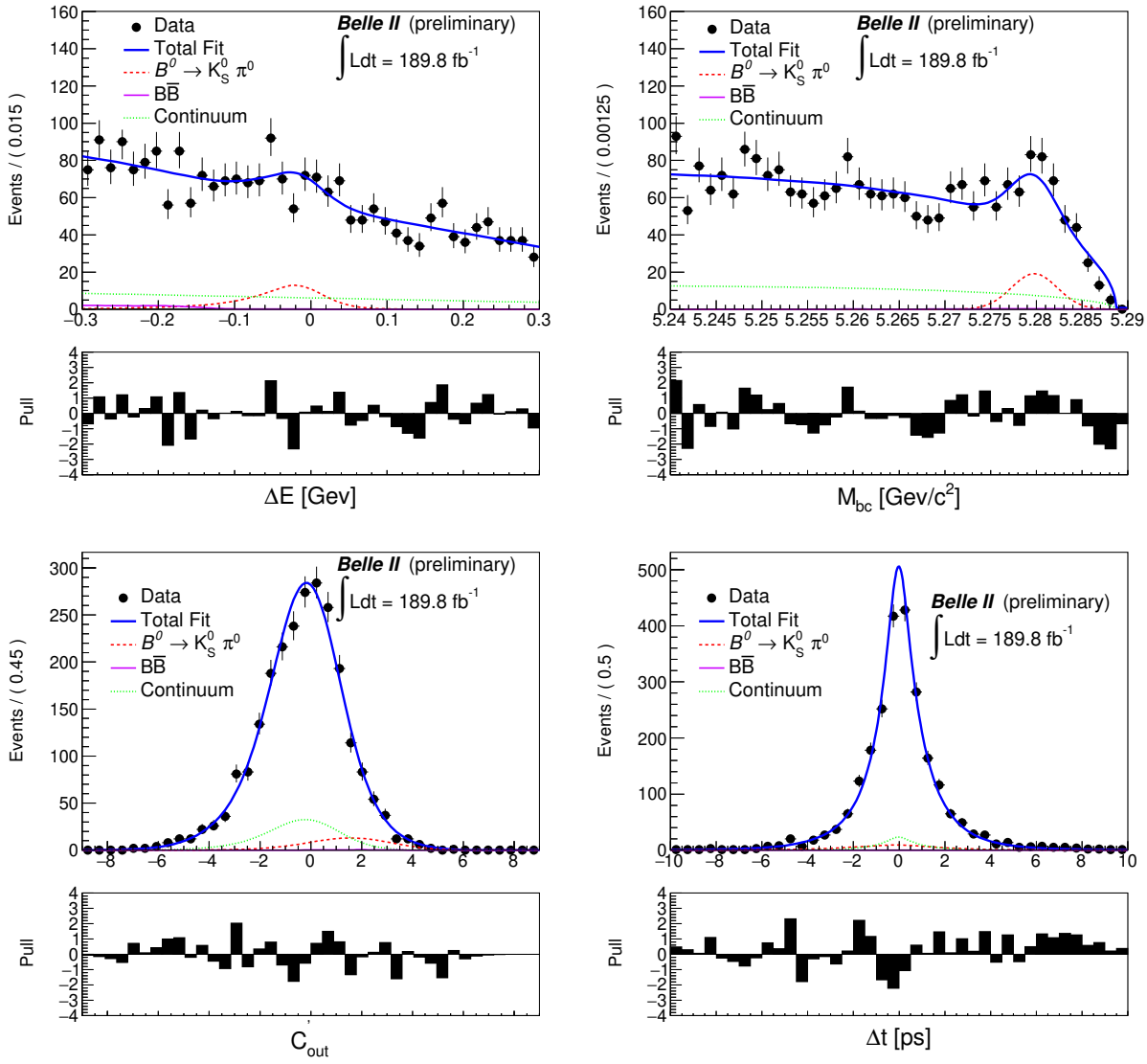

FIG. 3. Signal enhanced 4D fit projections for $q \cdot r$ integrated sample.

5. SYSTEMATIC UNCERTAINTIES

We consider systematic uncertainties arising from several potential sources. Summary of systematic uncertainties contributing to the branching fraction and CP asymmetry parameters are reported in Table I and II, respectively. We assume the sources to be independent and add them in quadrature to get the total systematic uncertainty.

5.1. Systematic uncertainties for the branching fraction

- **Tracking efficiency**

  The systematic uncertainty associated with possible data-MC discrepancies in the reconstruction of charged particles is 0.30% for per track[23]. We linearly add an uncertainty corresponding to each of the two pion tracks originating from the K_S^0 decay in the signal side.

- **K_S^0 reconstruction efficiency**

  From a data-MC comparison we observe that the ratio of K_S^0 reconstruction efficiency changes approximately linearly as a function of the flight distance [23]. We apply an uncertainty of 0.40% for each centimeter of average flight length of the K_S^0 candidate resulting in a 4.2% total systematic uncertainty.

- **π^0 reconstruction efficiency**

  We estimate the systematic uncertainty due to possible data-MC discrepancies in the π^0 reconstruction and selection using inclusive decay samples of $D^0 \to K^-\pi^+\pi^0$ and $D^0 \to K^-\pi^+$. The data-MC efficiency ratio is found to be close to unity with an uncertainty of 7.5%, which we allocate as the systematic uncertainty.

- **Continuum suppression efficiency**

  We evaluate possible data-simulation discrepancies in the continuum-suppression distributions using the control channel $B^+ \to \overline{D}^0(\to K^+\pi\pi^0)\pi^+$. Since the ratio of selection efficiency obtained in data and MC is close to 1, the statistical uncertainty (1.6%) on the efficiency ratio is assigned as the systematic uncertainty.

- **$B\overline{B}$ pair counting**

  An overall uncertainty of 3.2% is taken as a systematic uncertainty on the number of $B\overline{B}$ used [24], which includes the uncertainty on f^{00}, cross section, integrated luminosity, and potential shifts from the peak CM energy during the run periods.

- **Signal and background modeling**

  The uncertainties due to signal PDF shape are estimated by varying the correction factors by $\pm 1\sigma$ of their statistical uncertainty. Similarly, the uncertainties due to background PDF shape are calculated by varying all fixed parameters by $\pm 1\sigma$, determined from MC component fit.

- **Possible fit bias**

  A potential fit bias is checked by performing an ensemble test comprising 1000 pseudoexperiments in which signal events are drawn from the corresponding MC sample and background events are generated according to their PDF shapes. We calculate the mean shift of signal yield from the input value and assign it as a systematic uncertainty.

- **Physics parameters** Physics parameters τ_{B^0}, Δm_d and $\mathcal{S}_{CP}$ are fixed to the world average in *CP* fit. Therefore, the systematic uncertainty is estimated by varying their error by $\pm 1\sigma$.

TABLE I. List of systematic uncertainties contributing to the measured branching fraction.

Source	$\delta\mathcal{B}(\%)$
Tracking efficiency	0.6
K^0_S reconstruction efficiency	4.2
π^0 reconstruction efficiency	7.0
Continuum suppression efficiency	1.6
Number of $B\overline{B}$ events	3.2
Signal model	1.0
Continuum background model	0.9
Possible fit bias	2.0
Physics parameters	0.4
Total	9.3

5.2. Systematic uncertainties on the $\mathcal{A}_{CP}$

- **Flavor tagging**

  Systematic error due to uncertainties in the wrong tag fractions is estimated by varying the parameters individually for each r region within its statistical and systematical variations.

- **Resolution function**

  Systematic error due to uncertainties in the resolution function is estimated by varying each resolution parameter obtained from data by $\pm 1\sigma$ considering both of statistical and systematical variations.

- **Physics parameters** Physics parameters τ_{B^0}, Δm_d and $\mathcal{S}_{CP}$ are fixed to the world average in CP fit. Therefore, the systematic uncertainty is estimated by varying their error by $\pm 1\sigma$.

- ***B* decay background asymmetry**

  In the nominal fit, we assume the charmless B decay background to be CP symmetric. However, there could be a nontrivial asymmetry arising due to this component. To take such possibility into account, we use an alternative Δt PDF given by

$$P_{B\bar{B}}(\Delta t, q) = \frac{\mathrm{e}^{-|\Delta t|/\tau_{B^0}}}{4\tau_{B^0}}[1 + q\{\mathcal{A}_{CP}\cos(\Delta m_d \Delta t) + \mathcal{S}_{CP}\sin(\Delta m_d \Delta t)\}] \otimes R_{B\bar{B}}, \quad (7)$$

  instead of RooDecayPDF. We perform two different fits by setting S_{CP} to either $+1$ or -1 and $\mathcal{A}_{CP} = 0.0$. We then calculate the deviations in $\mathcal{A}_{CP}$ and $\mathcal{S}_{CP}$ values from the nominal fit. These deviations are assigned as a systematic uncertainty due to B decay background asymmetry. We estimate this systematic in $B^0 \to J/\psi K^0_S$ data itself.

- **Possible fit bias**

  A potential fit bias is checked by performing an ensemble test comprising 1000 pseudoexperiments in which signal events are drawn from the corresponding MC sample

and background events are generated according to their PDF shapes. We calculate the mean shift of $\mathcal{A}_{CP}$ and $\mathcal{S}_{CP}$ from the input value and assign it as a systematic uncertainty.

- **Tag-side interference**

  Systematic uncertainties arises due to the tag-side interference is taken from Ref. [25].

- **Signal and background modeling**

  The uncertainties due to signal and background PDF shape are estimated in a manner similar to the branching fraction case.

- **Vertex reconstruction (including VXD misalighnment)**

  The systemaric uncertainty is taken from Ref. [26].

TABLE II. List of systematic uncertainties contributing to $\mathcal{A}_{CP}$.

Source	$\delta\mathcal{A}_{CP}$
Flavor tagging	0.040
Resolution function	0.050
Physics parameter	0.021
B decay background asymmetry	0.002
Possible fit bias	0.010
Tag-side interference	0.008
Background modeling	0.004
Signal modeling	0.015
Vertex reconstruction	0.033
Total	0.076

6. RESULT AND SUMMARY

We report measurements of the branching fraction and direct CP asymmetry ($\mathcal{A}_{CP}$) based on 189.8 fb^{-1} data sample collected at the $\Upsilon(4S)$ resonance by the Belle II detector. The observed signal yield is 135^{+16}_{-15}. We measure $\mathcal{A}_{CP} = -0.41^{+0.30}_{-0.32}(\text{stat}) \pm 0.08(\text{syst})$ and $\mathcal{B}(B^0 \to K^0\pi^0) = [11.0 \pm 1.2(\text{stat}) \pm 1.0(\text{syst})] \times 10^{-6}$. This is the first measurement of $\mathcal{A}_{CP}$ in $B^0 \to K^0\pi^0$ decays reported by Belle II with a time-dependent CP violation analysis framework. The results agree with previous determinations and show a detector performance comparable with the best Belle results.

7. ACKNOWLEDGEMENT

We thank the SuperKEKB group for the excellent operation of the accelerator; the KEK cryogenics group for the efficient operation of the solenoid; the KEK computer group for on-site computing support; and the raw-data centers at BNL, DESY, GridKa, IN2P3, and INFN

for off-site computing support. This work was supported by the following funding sources: Science Committee of the Republic of Armenia Grant No. 20TTCG-1C010; Australian Research Council and research grant Nos. DP180102629, DP170102389, DP170102204, DP150103061, FT130100303, FT130100018, and FT120100745; Austrian Federal Ministry of Education, Science and Research, Austrian Science Fund No. P 31361-N36, and Horizon 2020 ERC Starting Grant no. 947006 "InterLeptons"; Natural Sciences and Engineering Research Council of Canada, Compute Canada and CANARIE; Chinese Academy of Sciences and research grant No. QYZDJ-SSW-SLH011, National Natural Science Foundation of China and research grant Nos. 11521505, 11575017, 11675166, 11761141009, 11705209, and 11975076, LiaoNing RevitaJHEP 10 (2014) 165lization Talents Program under contract No. XLYC1807135, Shanghai Municipal Science and Technology Committee under contract No. 19ZR1403000, Shanghai Pujiang Program under Grant No. 18PJ1401000, and the CAS Center for Excellence in Particle Physics (CCEPP); the Ministry of Education, Youth and Sports of the Czech Republic under Contract No. LTT17020 and Charles University grants SVV 260448 and GAUK 404316;

European Research Council, 7th Framework PIEF-GA-2013-622527, Horizon 2020 ERC-Advanced Grants No. 267104 and 884719, Horizon 2020 ERC-Consolidator Grant No. 819127, Horizon 2020 Marie Sklodowska-Curie grant agreement No. 700525 'NIOBE,' and Horizon 2020 Marie Sklodowska-Curie RISE project JENNIFER2 grant agreement No. 822070 (European grants); L'Institut National de Physique Nucléaire et de Physique des Particules (IN2P3) du CNRS (France); BMBF, DFG, HGF, MPG, and AvH Foundation (Germany); Department of Atomic Energy under Project Identification No. RTI 4002 and Department of Science and Technology (India); Israel Science Foundation grant No. 2476/17, United States-Israel Binational Science Foundation grant No. 2016113, and Israel Ministry of Science grant No. 3-16543; Istituto Nazionale di Fisica Nucleare and the research grants BELLE2; Japan Society for the Promotion of Science, Grant-in-Aid for Scientific Research grant Nos. 16H03968, 16H03993, 16H06492, 16K05323, 17H01133, 17H05405, 18K03621, 18H03710, 18H05226, 19H00682, 26220706, and 26400255, the National Institute of Informatics, and Science Information NETwork 5 (SINET5), and the Ministry of Education, Culture, Sports, Science, and Technology (MEXT) of Japan;

National Research Foundation (NRF) of Korea Grant Nos. 2016R1D1A1B01010135, 2016R1D1A1B02012900, 2018R1A2B3003643, 2018R1A6A1A06024970, 2018R1D1A1B-07047294, 2019K1A3A7A09033840, and 2019R1I1A3A01058933, Radiation Science Research Institute, Foreign Large-size Research Facility Application Supporting project, the Global Science Experimental Data Hub Center of the Korea Institute of Science and Technology Information and KREONET/GLORIAD; Universiti Malaya RU grant, Akademi Sains Malaysia and Ministry of Education Malaysia; Frontiers of Science Program contracts FOINS-296, CB-221329, CB-236394, CB-254409, and CB-180023, and SEP-CINVESTAV research grant 237 (Mexico); the Polish Ministry of Science and Higher Education and the National Science Center; the Ministry of Science and Higher Education of the Russian Federation, Agreement 14.W03.31.0026, and the HSE University Basic Research Program, Moscow; University of Tabuk research grants S-0256-1438 and S-0280-1439 (Saudi Arabia); Slovenian Research Agency and research grant Nos. J1-9124 and P1-0135;

Agencia Estatal de Investigacion, Spain grant Nos. FPA2014-55613-P and FPA2017-84445-P, and CIDEGENT/2018/020 of Generalitat Valenciana; Ministry of Science and Technology and research grant Nos. MOST106-2112-M-002-005-MY3 and MOST107-2119-M-002-035-MY3, and the Ministry of Education (Taiwan); Thailand Center of Ex-

cellence in Physics; TUBITAK ULAKBIM (Turkey); Ministry of Education and Science of Ukraine; the US National Science Foundation and research grant Nos. PHY-1807007 and PHY-1913789, and the US Department of Energy and research grant Nos. DE-AC06-76RLO1830, DE-SC0007983, DE-SC0009824, DE-SC0009973, DE-SC0010073, DE-SC0010118, DE-SC0010504, DE-SC0011784, DE-SC0012704, DE-SC0021274; and the Vietnam Academy of Science and Technology (VAST) under grant DL0000.05/21-23.

8. REFERENCES

[1] E. Kou et al. (Belle II Collaboration), PTEP **2019**, 123C01 (2019), arXiv-1808.10567.
[2] N. Cabibbo, Phys. Rev. Lett. **10**, 531 (1963); M. Kobayashi and T. Maskawa, Prog. Theor. Phys. **49**, 652 (1973).
[3] M. Gronau, Phys. Lett. B **627**, 82 (2005).
[4] F. Abudinén et al. (Belle II Collaboration), arXiv-2110.00790.
[5] Y. Chao et al. (Belle Collaboration), Phys. Rev. D **69**, 111102 (2004).
[6] K. F. Chen et al. (Belle Collaboration), Phys. Rev. D **72**, 012004 (2005).
[7] B. Aubert et al. (BaBar Collaboration), Phys. Rev. Lett. **93**, 131805 (2004).
[8] B. Aubert et al. (BaBar Collaboration), Phys. Rev. D **71**, 111102 (2005).
[9] Y. Amhis et al. (Heavy Flavor Averaging Group), Eur. Phys. J. C (2021) 81:226, arXiv:1909.12524.
[10] T. Abe et al. (Belle II Collaboration), arXiv:1011.0352 (2010).
[11] K. Akai, K. Furukawa, and H. Koiso (SuperKEKB Group), Nucl. Instrum. Meth. A **907**, 188 (2018).
[12] D. Lange, Nucl. Instrum. Meth. A **462**, 152 (2001).
[13] E. Barberio et al., Comp. Phys. Comm. **66**, 115 (1991).
[14] B. Ward, S. Jadach and Z. Was, Nucl. Phys. B Proc. Suppl. **116**, 73 (2003)
[15] T. Sjöstrand et al., Comp. Phys. Comm. **178**, 852 (2008).
[16] S. Agostinelli et al., Nucl. Instrum. Meth. A **506**, 250 (2003).
[17] T. Keck et al., arXiv:1609.06119 (2016).
[18] F. Abudinén et al. (Belle II Collaboration), arXiv:2110.00790
[19] T. Skwarnicki, PhD thesis, INP Krakow, DESY-F31-86-02 (1986).
[20] H. Albrecht et al. (ARGUS Collaboration), Phys. Lett. B **241**, 278 (1990).
[21] K. S. Cranmer, Comp. Phys. Commun. **136**, 198 (2001).
[22] F. Abudinén et al. (Belle II Collaboration), arXiv:2104.14871 (2021).
[23]
[24] `https://indico.belle2.org/event/5891/contributions/31643/attachments/15000/22539/Bcounting_B2GM_Jan2022_v2.pdf`
[25] I. Adachi et al. (Belle Collaboration), Phys. Rev. Lett. **108**, 171802 (2012)
[26] L. ˇSantelj et al. (Belle Collaboration), JHEP **10** (2014) 165.